I&EC research
Industrial & Engineering Chemistry Research
pubs.acs.org/IECR
Article

Ether-Linked Diamine Carboxylate Ionic Liquid Aqueous Solution for Efficient Absorption of SO_2

Bin Jiang, Shuai Hou, Luhong Zhang, Na Yang, Na Zhang, Xiaoming Xiao, Xiaodong Yang, Yongli Sun, and Xiaowei Tantai*

Cite This: *Ind. Eng. Chem. Res.* 2020, 59, 16786−16794

ABSTRACT: Ionic liquids (ILs) as promising absorbents for SO_2 capture in flue gas desulfurization have been extensively studied. In this work, a multisite absorption strategy was used to synthesize ether-linked diamine protic ionic liquids (EDPILs) for efficient SO_2 capture. The prepared EDPILs containing ether-linkage chain exhibited superior SO_2 absorption relative to conventional protic ionic liquids (PILs). Density functional theory calculations demonstrated that the ether-linkage chain intensified the physical interaction between EDPILs and SO_2. In a subsequent experiment, bis(2-dimethylaminoethyl) ether dilactate $[BDMAEE][L]_2$, which possessed outstanding SO_2 capture capacities, was used to prepare aqueous solutions (aq), which reduced viscosity of PILs and improved their applicability. An in-depth assessment of the desulfurization performance of $[BDMAEE][L]_2$ aq revealed that effective SO_2 absorption can be achieved even at relatively low concentrations. Specifically, 50 wt % $[BDMAEE][L]_2$ aq exhibited a high absorption capacity (1.04 mol_{SO_2}/mol_{ILs}, 0.097 $g_{SO_2}/g_{absorbents}$) as well as a high SO_2/CO_2 selectivity at 0.2 vol % SO_2 and 40 °C. Overall, ether-linked absorbents with improved desulfurization performance (high SO_2 absorption capacity, satisfactory SO_2 removal efficiency, and excellent reusability) possess good application prospects in flue gas desulfurization.

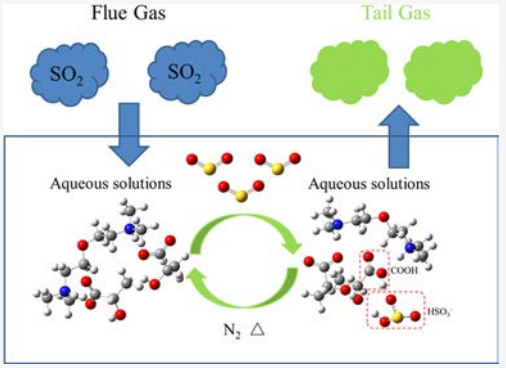

1. INTRODUCTION

Sulfur dioxide (SO_2), a hazardous air pollutant generated by fossil fuel combustion, is highly harmful to human health and to the environment.[1,2] Conventionally, SO_2 emission is reduced through flue gas desulfurization (FGD).[3] Commercial technologies like lime/limestone process[4,5] and ammonia scrubbing process[6] are used for FGD. However, these methods have various limitations, including the use of nonrecyclable absorbents, generation of a large amount of low-value byproducts, and wastewater.[7,8] Additionally, ammonia scrubbing process leads to secondary pollution due to ammonia escape.[6,9] Thus, novel absorbents that reversibly absorb SO_2 are needed for the FGD process.

Recently, ionic liquids (ILs), with negligible vapor pressure, nonflammability, and tunable properties,[10−12] have been widely investigated as alternative absorbents for efficient acid gas absorption.[13−16] In SO_2 absorption, ILs exhibit high desulfurization efficiency; they are unaffected by SO_2 concentration and can be regenerated without secondary pollution. Protic ionic liquids (PILs), among the ILs developed for SO_2 capture,[17−19] are the most preferred in commercial applications due to their relatively simple preparation procedures. Han[20] reported that tetramethylguanidinium lactate [TMG][L] effectively absorbed SO_2 with a loading capacity of up to 0.978 mol_{SO_2}/mol_{ILs} at 40 °C and 8 vol % SO_2. Shang[21] synthesized three guanidinium-based PILs for SO_2 capture, which possessed high absorption rates, with SO_2 absorption capacities ranging from 2.24 to 3.16 mol_{SO_2}/mol_{ILs}. However, PILs have inherent limitations that curtail their use in industrial scale, including ultrahigh viscosity and high cost.

To overcome these shortcomings, a novel method, in which low-cost PILs are blended with water to prepare PILs aq,[22] has been proposed. Wu[23] found that triethylenetetramine tetralactate ($[TETA][L]_4$) aq exhibited high SO_2 absorption with excellent reversibility. Moreover, Huang[24] synthesized a series of hydroxylammonium dicarboxylate ionic liquids and then mixed them with free *N*,*N*-dimethylethanolamine (DMEA) and water. The absorbents exhibited low viscosities and rapid SO_2 absorption rates. We have previously reported a class of novel diamine polycarboxylate protic ionic liquids (DPPILs) aq, which can be utilized for the removal of SO_2, in which 50 wt %*N*,*N*-dimethylethylenediamine citrate [DMEDA][CA] aq achieved a high SO_2 removal efficiency.[25] According to previous studies, PILs synthesized from weak

Received: June 9, 2020
Revised: August 18, 2020
Accepted: August 24, 2020
Published: August 24, 2020

acids with pK_a values >1.8 have been found to efficiently absorb low concentrations of SO_2 from flue gas.[26] Moreover, considering that SO_2 desorption is a high-temperature process (occurring at 100−120 °C for organic amine scrubbing),[27] the thermostabilities and volatilities of PILs should be further optimized to meet the condition. Thus, weak acids with appropriate acidity and low vapor pressure should be used to synthesize PILs for industrial application.[28] Moreover, appropriate modification of the molecular structure of PILs is necessary for improved thermal stability.

Multisite PILs with specific molecular structures exhibit outstanding SO_2 absorption−desorption performance[25] and excellent stability during absorption−desorption cycles,[28,29] which are suitable for SO_2 absorption. Ether-functionalized ILs have attracted immense attention due to superior physical and chemical properties like high biodegradability,[30] high thermal stability,[31] and low viscosity.[13] As a functional group with appropriate Lewis alkalinity, the ether group achieves efficient and recyclable SO_2 absorption by moderate physical interaction.[18] Thus, it is deduced that ether-linked diamine protic ionic liquids (EDPILs) exhibit excellent SO_2 absorption performance. However, EDPILs aq employed for SO_2 absorption have not been studied so far. More specifically, the use of quantum chemical calculations to systematically clarify the molecular interactions between ether group and SO_2 has not been sufficiently investigated.

In this work, we describe a novel strategy to synthesize new EDPILs using low-cost and readily available reagents (their structures are shown in Scheme 1), efficiently improving SO_2 absorption performance. The contributions of ether-linkage chain to desulfurization performance were theoretically and experimentally investigated. We then prepared EDPIL aqueous solutions by blending $[BDMAEE][L]_2$ with water. The physical properties of the solutions, including density and viscosity, were measured. The effects of $[BDMAEE][L]_2$ concentration, temperature, and SO_2 concentration on SO_2 absorption were also evaluated. The SO_2/CO_2 selectivity, SO_2 removal efficiency, and reversibility of the studied absorbent in simulated flue gas were tested. The mechanism of interaction between $[BDMAEE][L]_2$ aq and SO_2 was examined by spectroscopic characterization and quantum chemical calculations.

Scheme 1. Structures of Diamine and Lactic Acid for IL Synthesis

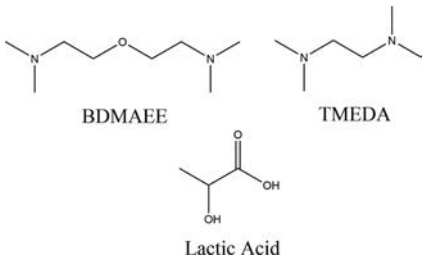

2. EXPERIMENTAL SECTION

2.1. Materials. Bis(2-dimethylaminoethyl) ether (BDMAEE) (99%) and tetramethylethylenediamine (TMEDA) (99%) were purchased from Aladdin Industrial Corporation. Lactic acid (99.7%) was purchased from Tianjin Kemiou Chemical Reagent Co., Ltd (Tianjin, China). SO_2 (99.9%), N_2 (99.99%), and CO_2 (99.99%) were purchased from Tianjin Dongxiang Specialty Gases Co., Ltd (Tianjin, China).

2.2. Preparation of Absorbents. EDPILs were synthesized using previously described methods.[23,32] As an example, to synthesize $[BDMAEE][L]_2$, 0.1 mol of BDMAEE was dissolved in 50 mL of deionized water. The solution was then transferred into a 250 mL three-neck flask equipped with a reflux condenser in an ice−water bath and vigorously stirred with a magnetic stirrer. Lactic acid (0.2 mol) was then dissolved in 100 mL of deionized water, loaded into a dropping funnel, and added into the solution dropwise for 2 h. The solution was left to react for 24 h at 0 °C. The solvent (water) was removed by evaporation under vacuum at 80 °C to obtain the crude EDPILs. The EDPIL was then vacuum-dried at 80 °C for 48 h and then mixed with deionized water at the indicated mass ratios (Table S2) to prepare EDPILs aq.

2.3. Characterization. EDPIL structures were characterized by ^{1}H NMR using a 500 MHz spectrometer (Bruker Avance III, Germany), and the results are presented in the Supporting Information. The densities of the absorbents were measured at 25 °C using a 5 cm^3 pycnometer (with ±2.5% deviation) and precalibrated with distilled water. The absorbents were then measured in pentaplicates, and average values were used for analyses. A Brookfield DV-II + Pro viscometer, precalibrated with standard silicone oil at 25 °C, was used to determine viscosities of the absorbents. Each absorbent was tested five times, and the mean values were calculated. Deviations of the measurements were estimated to be less than ±5%. The absorption mechanism was expounded using FTIR (Bruker, TENSOR II, Germany). The residual water in PILs significantly influences their absorption performance, and the water content of the PILs was measured to be <0.5 wt % (Table S1) using a Karl Fischer moisture titrator (AKF-2010, Hogon Co., Ltd.). Thermogravimetric analysis (TGA, NETZSCH) was conducted to explore the thermostability of the prepared PILs, and the decomposition temperatures, corresponding to 5% weight loss, of PILs were all above 148 °C (Figure S1). This indicated that they were sufficiently stable during SO_2 absorption−desorption cycles. Additionally, owing to the extremely low water content of PILs, the slight weight loss before 100 °C may result from the relatively poor thermal stability of lactate anions. The TGA curve of lactic acid is shown in Figure S1.

2.4. Absorption and Desorption of SO_2. The absorption and desorption experiments were carried out using previously reported methods.[25,33] The schematic diagram of the absorption−desorption system is shown in Figure 1.

In a typical absorption process, 100 mL/min simulated flue gas (2 vol % SO_2 and 98 vol % N_2) was consecutively bubbled through two absorption tubes loaded with 2 g of deionized water (to offset the water loss) and absorbents. The tubes were partially immersed into a constant-temperature water bath. Mass flowmeters were used to control the concentration of SO_2 in the simulated flue gas by adjusting the flow rate ratios of SO_2 and N_2. The loading capacity of SO_2 was determined by the iodine titration method (HJ/T 56-2000, a standard method of the State Environmental Protection Administration of China). Furthermore, to examine the desulfurization performance of the absorbents, absorption experiments for the simulated flue gas (low SO_2 concentrations, 0.2−0.4 vol %) were conducted by loading 2 g of absorbent into the absorption tube. The concentration of SO_2 at the inlet and

https://dx.doi.org/10.1021/acs.iecr.0c02877
Ind. Eng. Chem. Res. 2020, 59, 16786−16794

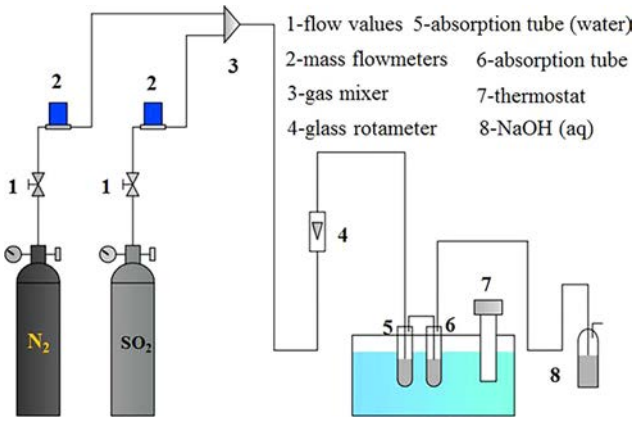

Figure 1. Schematic diagram of the absorption−desorption experiment system.

outlet of the absorption tube was determined using a flue gas analyzer (Testo 350), and the deviations induced by the instrument were estimated to be ±5% (0.01−0.5 vol %) and ±0.0005 vol % (0−0.0099 vol %) following the instructions in Testo 350. Next, we determined the SO_2 removal efficiency (RE) as follows:

$$RE = (C_{in} - C_{out})/C_{in} \times 100\% \quad (1)$$

where C_{in} and C_{out} represented the inlet and outlet SO_2 concentrations, respectively.

In the desorption experiment, 100 mL/min pure N_2 was used to sweep SO_2 saturated absorbents (corresponding to 2 g of virgin absorbent) at 100 °C. All experiments were conducted in triplicate. The estimated uncertainty of SO_2 loading capacity was less than ±5%.

3. RESULTS AND DISCUSSION

3.1. Absorption and Desorption of SO_2 by the PILs. The effect of the ether-linkage chain on the SO_2 absorption−desorption performance of the PILs was systematically investigated. The absorption−desorption experiments[34] were conducted at 40 °C, 100 vol % SO_2 at 50 mL/min, and 100 °C, 100 vol % N_2 at 100 mL/min. Gas conditions were optimized through preliminary experiments. First, the absorption rate of SO_2 was estimated from the slope of the absorption curves.[35] As shown in Figure 2, the EDPILs containing ether-linkage chains presented abrupt slopes, reflecting more rapid absorption kinetics relative to conventional PILs. Additionally, the saturated loading capacities of [BDMAEE][L] and [BDMAEE][L]$_2$ were 2.259 and 2.621 mol_{SO_2}/mol_{ILs}, respectively. Of note, these values were higher than those of [TMEDA][L] and [TMEDA][L]$_2$ (1.552 and 1.768 mol_{SO_2}/mol_{ILs}, respectively). This suggested that absorption capacity can be efficiently enhanced through multisite absorption based on the ether-linkage chain. While [TMEDA][L] solidified during absorption, [BDMAEE][L] remained in liquid form. This may be because [BDMAEE][L] with ether-linkage chains was more flexible than [TMEDA][L],[36] which prevented the formation of complex hydrogen-bond networks like [TMEDA][L] in the absorption. As a result, the ether-linkage chain improved the physical properties of the absorbents. Moreover, [TMEDA][L]$_2$ exhibited good flow properties along with a higher mass transfer efficiency, which resulted in superior absorption capacities to [TMEDA][L].

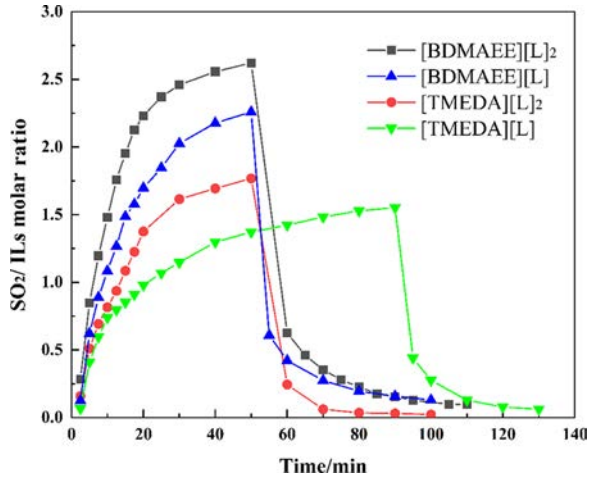

Figure 2. SO_2 absorption capacities and desorption residues of various absorbents.

Concerning SO_2 desorption, the PILs achieved almost total desorption, reaching similarly low desorption residues. However, due to their superior absorption capacities, EDPILs took longer to reach the same desorption residue as the conventional PILs. Remarkably, the available absorption capacity is usually important in selecting absorbents, which has been regarded as a significant index in previous reports.[37] It is calculated as the difference between absorption capacity and desorption residue. The available absorption capacity of EDPILs exceeded that of conventional PILs. For instance, the molar available absorption capacity of [BDMAEE][L] was as high as 2.129 mol_{SO_2}/mol_{ILs}, while that of [TMEDA][L] was 1.490 mol_{SO_2}/mol_{ILs}. Relative to conventional PILs without the ether-linkage chain, EDPILs exhibited superior SO_2 capture capacities due to the following factors: (1) the electronegative oxygen provided extra interaction sites, which improved SO_2 absorption performance of the EDPILs via physical interaction[38] and (2) the weak physical interaction between ether groups and SO_2 efficiently overcame desorption difficulty.[39] Thus, ether-linkage chains improved SO_2 capture performance of EDPILs. In the next section, the interaction between the PILs and SO_2 was further explored at the molecular level through quantum chemical calculations.

3.2. Quantum Chemical Calculations. To theoretically determine how the ether-linkage chain affected SO_2 absorption, quantum chemical calculations were completed using Gaussian 09 program[40,41] on the B3LYP/6-311+G(d,p) level.[42−44] Details of the methods employed in the quantum chemical calculations are provided in the Supporting Information. Structures of [BDMAEE][L] and [TMEDA]-[L]-$n$$SO_2$ (n = 1, 2, and 3) are shown in Figure 3. The interaction energies were −67.832, −116.078, and −134.496 kJ/mol for 1:1, 1:2, and 1:3 ([BDMAEE][L]:SO_2) absorption, respectively. The high interaction energies of [BDMAEE][L]-SO_2 and [BDMAEE][L]−2SO_2 complexes confirmed the strong chemical interactions between [BDMAEE][L] and the first two SO_2 molecules. Importantly, the third SO_2 molecule interacted with the ether group on the $[BDMAEE]^+$ cation. The intermolecular O···S distance was 2.72 Å, and the interaction energy was approximately −18.418 kJ/mol, indicating the existence of physical interaction after absorption. Additionally, it was conclusive from our findings that the ether-linkage chain may induce strong physical interaction between

https://dx.doi.org/10.1021/acs.iecr.0c02877
Ind. Eng. Chem. Res. 2020, 59, 16786−16794

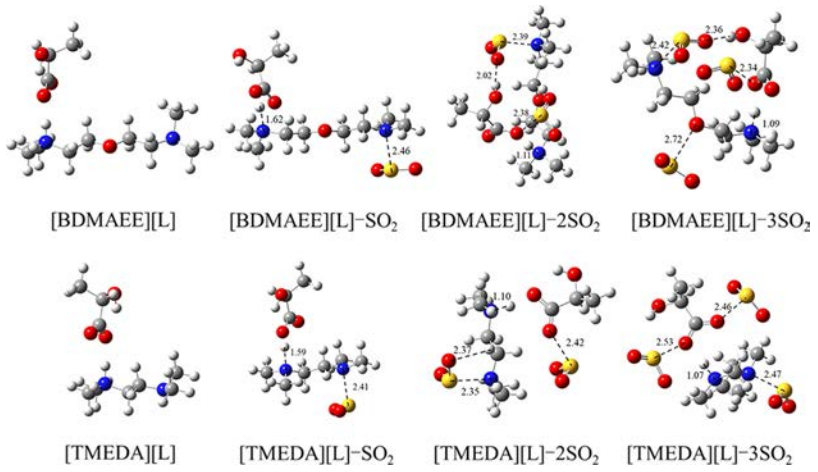

Figure 3. Optimized structures of the PILs, PILs-SO_2, PILs-$2SO_2$, and PILs-$3SO_2$ complexes.

EDPILs and SO_2. In the [BDMAEE][L]−$2SO_2$ complex, SO_2 interacted with the hydrogen atom on the hydroxyl group of lactate via strong hydrogen bonding (S═O···H-O). Distinctly, the O atom of SO_2 engendered a weak hydrogen bond with the H atom of C−H (S═O···H-C) on [TMEDA][L]−$2SO_2$. The lengths of the hydrogen bonds were 2.02 and 2.37 Å, corresponding to approximately 25.7 and 12.9% reduction in the total van der Waals radii of the two interacting O and H atoms.[45] Their corresponding binding energies were −116.078 and −107.287 kJ/mol. Thus, the ether-linkage chain moderately increased the affinity of EDPILs for the SO_2 molecule by consolidating physical interaction, thereby facilitating SO_2 absorption and desorption. Results from quantum chemical calculations were consistent with findings from the above experiments. Thus, [BDMAEE][L] absorbed SO_2 synergistically through chemical and physical interactions.

3.3. Absorption Isotherm and Absorption Enthalpy of SO_2 by PILs. *3.3.1. Absorption Isotherm Curves of PILs.* To further evaluate the performance of the absorbents, the SO_2 absorption capacities of $[BDMAEE][L]_2$ and $[TMEDA][L]_2$ at 40 °C were plotted against different SO_2 concentrations, as shown in Figure S2. Results showed that all absorption isotherm curves were similar to the nonideal Langmuir-type profiles. The loading capacity of SO_2 increased rapidly with increasing concentration of SO_2 in the low-concentration region and then increased almost linearly in the high-concentration region. These results indicated that PILs effectively captured SO_2 through strong chemical interactions in the low-concentration region. Moreover, physical absorption played an important role in the high-concentration region. Furthermore, it was observed that $[BDMAEE][L]_2$ exhibited superior SO_2 absorption capacity relative to $[TMEDA][L]_2$, and the differences in absorption capacity between the two absorbents were more conspicuous in the high-concentration region. Concretely, the absorption capacity of $[BDMAEE][L]_2$ for 100 vol % SO_2 was 2.621 mol_{SO_2}/mol_{IL}, while that of $[TMEDA][L]_2$ was 1.768 mol_{SO_2}/mol_{IL}, with a difference of 0.853 mol_{SO_2}/mol_{IL}. However, the loading capacities of the two PILs for 10 vol % SO_2 were 0.898 and 1.029 mol_{SO_2}/mol_{IL}, indicating no marked differences between them. The results further demonstrated that the absorption behavior of SO_2 in the ether group was physical interaction, and it dominated the process in the high-concentration region.

3.3.2. SO_2 Absorption Enthalpy of PILs. Next, variations of SO_2 absorption enthalpy following modification of PILs molecules were determined to investigate the absorption behavior of SO_2 on the sites. This was achieved using the van't Hoff equation $\ln K = (-\Delta H/R) \times (1/T) + C$. The general steps were as follows: First, following the preconceived general reaction scheme PILs + $nSO_2 \leftrightharpoons$ PILs·nSO_2, the reaction equilibrium constant (K) was defined as follows:

$$K = \frac{[\text{PILs}\cdot n\text{SO}_2]}{[\text{PILs}]\cdot P_{\text{SO}_{2^n}}} = \frac{\text{capacity}}{(n - \text{capacity})\cdot P_{\text{SO}_{2^n}}}$$

The related experiments for calculating absorption enthalpy were carried out in 100 vol % SO_2 under atmospheric pressure; hence, we assume $P_{SO_2} = 1$, and the capacity was the SO_2 absorption capacity. Therefore, K at different temperatures was determined using the SO_2 absorption experimental data of PILs (Table S2). Subsequently, the absorption enthalpy was calculated by the linear fitting of $\ln K$ and $1/T$ (Figure S3). The absorption enthalpy of $[BDMAEE][L]_2$ was −74.743 kJ/mol, while that of $[TMEDA][L]_2$ was −42.734 kJ/mol, indicating a difference of 32.009 kJ/mol between the absorption enthalpies of the two absorbents, which can be ascribed to the following reasons: the ether group physically interacted with SO_2, and the $[BDMAEE]^{2+}$ containing the ether-linkage chain provided more spaces for hosting SO_2,[46] causing a big difference in the absorption enthalpies between the two absorbents. The relatively low absorption enthalpy indicated weaker chemical interactions between $[TMEDA][L]_2$ and SO_2, which led to the better desorption performance of the $[TMEDA][L]_2$ in the absorption−desorption experiments (Figure 2).

3.4. Absorption of SO_2 by $[BDMAEE][L]_2$ aq. Based on its outstanding absorption and desorption performance, $[BDMAEE][L]_2$ was selected for further studies. However, its viscosity was too high, making it unable to improve the efficiency of heat and mass transfers. Thus, we prepared different concentrations of $[BDMAEE][L]_2$ aq to further investigate the SO_2 absorption under various absorption conditions and determined the densities and viscosities of $[BDMAEE][L]_2$ aq at 25 °C (Table S3).

3.4.1. Effect of $[BDMAEE][L]_2$ Concentration on Absorption−Desorption. The impact of $[BDMAEE][L]_2$ concentration on absorption−desorption performance is shown in Figure 4. High absorption capacities indicated that the

https://dx.doi.org/10.1021/acs.iecr.0c02877
Ind. Eng. Chem. Res. 2020, 59, 16786−16794

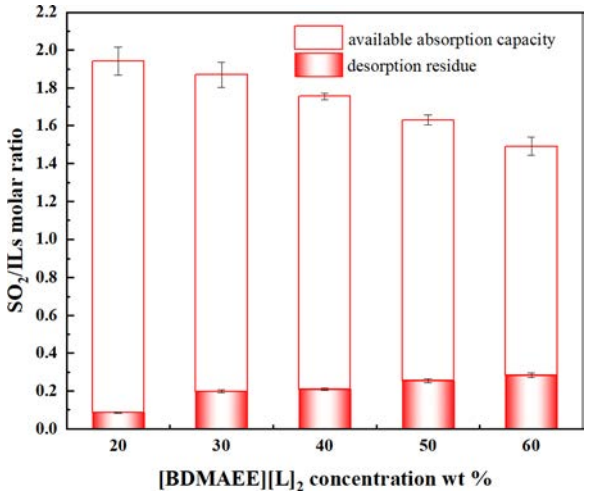

Figure 4. Molar available absorption capacities and desorption residues of $[BDMAEE][L]_2$ aq with various EDPIL concentrations at 20 °C and 2 vol % SO_2.

multisite strategy was effective for EDPILs aq. The saturated absorption capacities decreased with an increase in the concentration of $[BDMAEE][L]_2$. The absorption capacity of 20 wt % $[BDMAEE][L]_2$ aq was 1.943 mol_{SO_2}/mol_{ILs}, while that of 60 wt % $[BDMAEE][L]_2$ aq was 1.491 mol_{SO_2}/mol_{ILs}. Conversely, the desorption residues gradually increased with increasing concentration of $[BDMAEE][L]_2$. High concentration of $[BDMAEE][L]_2$ caused high absorbent viscosity (Table S3) along with low heat and mass transfer efficiencies, potentially reducing the desorption efficiency. Thus, the concentration of EDPILs in $[BDMAEE][L]_2$ aq significantly affected SO_2 absorption. During absorption, SO_2 in the simulated flue gas was dissolved and absorbed continuously. For this reason, the concentration of H_2SO_3 can be considered constant at various concentrations of $[BDMAEE][L]_2$ aq.[23] However, the concentrations of HSO_3^- and SO_3^{2-} decreased with the increase of water content in the absorbents. According to Le Chatelier's principle, the reversible reactions 4 and 5 (Figure 10) moved to the right, enhancing the $[BDMAEE][L]_2$ aq absorption performance.[23]

Figure 5 shows the available absorption capacities calculated from the experimental results. Notably, as the concentration of $[BDMAEE][L]_2$ increased from 20 to 60 wt %, the molar available absorption capacities linearly decreased from 1.856 to 1.207 mol_{SO_2}/mol_{ILs}. However, the gravimetric available absorption capacities were distinct from the molar available absorption capacities. Specifically, they increased sharply from 0.065 to 0.132 $g_{SO_2}/g_{absorbents}$ within a range of 20−50 wt %. When the concentration of $[BDMAEE][L]_2$ increased from 50 to 60 wt %, the gravimetric available absorption capacities remained almost constant. However, the viscosity of the studied absorbents increased by a factor of 2.30 (from 2.86 to 6.58 cP, Table S3). Generally, the gravimetric absorption capacity of absorbents is considered an essential property in the industrial application of absorbents, and we found that high concentrations of $[BDMAEE][L]_2$ enhanced the gravimetric absorption capacity. Nevertheless, ultrahigh concentration of $[BDMAEE][L]_2$ significantly enhanced viscosity, thereby reducing the heat and mass transfer efficiencies, and increased costs. We therefore selected 50 wt % $[BDMAEE][L]_2$ aq for further investigation.

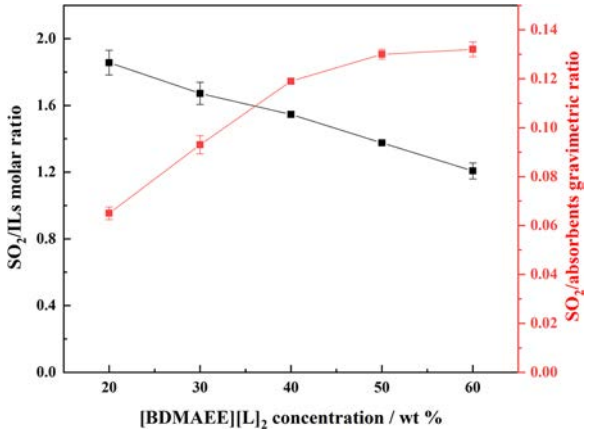

Figure 5. Available absorption capacities of $[BDMAEE][L]_2$ aq with various EDPIL concentrations at 20 °C and 2 vol % SO_2.

3.4.2. Effect of Temperature on SO_2 Absorption. The influence of temperature on SO_2 absorption by 50 wt % $[BDMAEE][L]_2$ aq is shown in Figure 6. The saturated SO_2 absorption capacity decreased rapidly as the temperature increased. Specifically, SO_2 absorption capacities decreased from 1.631 to 1.190 mol_{SO_2}/mol_{ILs} as the temperature increased from 20 to 60 °C, indicating that low temperatures favored SO_2 capture, and most of the absorbed SO_2 was stripped out by heating.

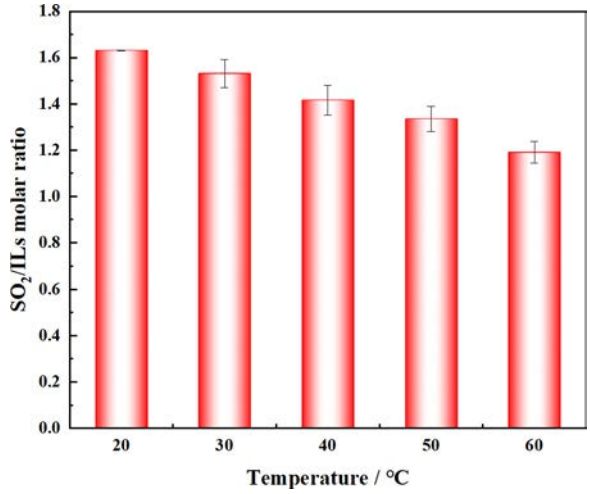

Figure 6. SO_2 absorption capacities of 50 wt % $[BDMAEE][L]_2$ aq at 2 vol % SO_2 and different temperatures.

3.4.3. Influence of SO_2 Concentration on Absorption. The SO_2 absorption capacity increased with the increase of SO_2 concentration at 40 °C (Figure 7). The saturated SO_2 absorption capacities increased from 1.416 mol_{SO_2}/mol_{ILs} at 2 vol % SO_2 to 2.815 mol_{SO_2}/mol_{ILs} at 100 vol % SO_2. This demonstrated that the concentration of SO_2 positively influenced absorption capacity. Subsequently, we examined the SO_2 absorption performance of the absorbent under standard FGD process conditions (0.2 vol % SO_2 and 40 °C). The saturated absorption capacity was still 1.04 mol_{SO_2}/mol_{ILs} (0.097 $g_{SO_2}/g_{absorbents}$), confirming that the studied absorbent

https://dx.doi.org/10.1021/acs.iecr.0c02877
Ind. Eng. Chem. Res. 2020, 59, 16786−16794

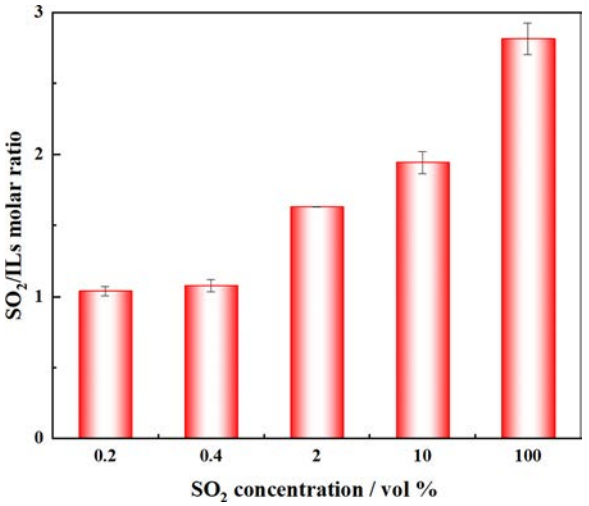

Figure 7. SO_2 absorption capacities of 50 wt % $[BDMAEE][L]_2$ aq at 40 °C and different concentrations of SO_2.

could efficiently absorb 0.2 vol % SO_2 from the flue gas under 40 °C. Furthermore, it was found that 50 wt % $[BDMAEE][L]_2$ aq exhibited a higher SO_2 absorption capacity (2.815 mol_{SO_2}/mol_{ILs}) relative to 50 wt % [DMEDA][CA] aq (1.760 mol_{SO_2}/mol_{ILs}) at 100 vol % SO_2 and 40 °C[25] even though the two absorbents have similar molecular structures. This suggested that the ether-linkage chain may contribute to SO_2 absorption in aqueous solutions via physical interaction.

To more comprehensively understand the studied absorbent, its SO_2 absorption capacities were compared to those of other ILs aq reported in the literature (Table 1). It was found that the studied absorbent had superior SO_2 absorption capacity relative to most ILs aq, especially at low SO_2 concentration, making it the more preferred and promising absorbent. Moreover, the absorbents prepared in this work were easily synthesized via a direct neutralization reaction without the need for organic solvents. Thus, the studied absorbent is cost-effective and suitable for FGD, while complying with the green chemistry principle and sustainable strategy.

In industrial applications, carbon dioxide (CO_2), an acidic gas present at high concentration in flue gas, interferes with SO_2 absorption. The SO_2/CO_2 selectivity of the 50 wt % $[BDMAEE][L]_2$ aq was also determined at 40 °C (Table S4). Surprisingly, the molar absorption capacity of SO_2 in 50 wt % $[BDMAEE][L]_2$ aq at 0.2 vol % SO_2 was 5.7 times higher than that of pure CO_2. This implied that $[BDMAEE][L]_2$ aq was highly selective for SO_2 and was thus suited for SO_2 capture. In the future study, we will investigate SO_2 selectivity of the absorbent in SO_2/CO_2 mixed simulated flue gas absorption experiments.

3.5. Absorption Mechanism. To thoroughly understand the interactions between EDPILs aq and SO_2 molecules, we characterized two absorbents, including unreacted $[BDMAEE][L]_2$ aq and SO_2 saturated $[BDMAEE][L]_2$ aq, using FTIR spectroscopy. The spectra are shown in Figure 8,

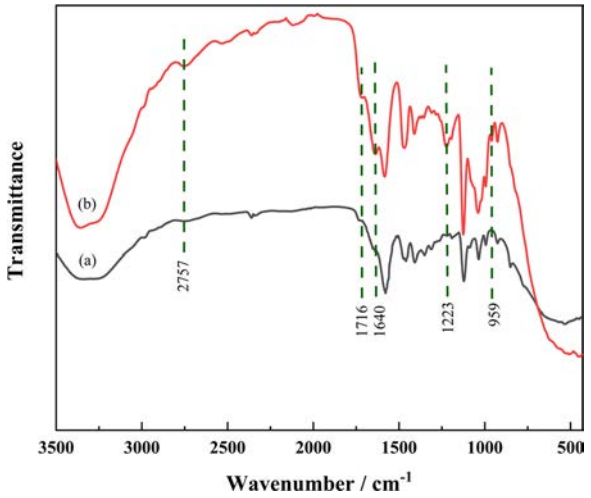

Figure 8. FTIR spectra of 50 wt % $[BDMAEE][L]_2$ aq before (a) and after (b) SO_2 absorption.

and more detailed FTIR spectra are shown in Figure S4. Relative to the FTIR spectrum of unreacted absorbent, five new characteristic peaks were found in the spectrum of the 100 vol % SO_2 saturated absorbent. The new peaks at 959 cm^{-1} were ascribed to the stretching vibrations of S−O bonds in SO_3^{2-}, HSO_3^-, or similar species.[48] This confirmed the chemical interactions between EDPILs aq and SO_2. The characteristic peak at 1223 cm^{-1} may be attributed to the symmetry stretching vibration of dissolved SO_2,[28] possibly emerging from the physical absorption of the ether-linkage chain. In addition, the new peaks at 1716 and 1640 cm^{-1} were

Table 1. Comparison of SO_2 Absorption Capacity between $[BDMAEE][L]_2$ aq and Other Absorbents

ILs aq	absorption (T, °C; SO_2, vol %)	absorption capability mol/mol[a]	absorption capability g/g[b]	ref
$[BDMAEE][L]_2$, 50 wt %	(40, 0.2)	1.040	0.097	this work
	(40, 2)	1.416	0.133	
	(20, 2)	1.631	0.153	
$[PEDETAH]_2[SO_4]$, 30 wt %	(40, 0.4)	0.677	0.045	28
[DMEDA][CA], 50 wt %	(40, 0.2)	0.34	0.039	25
	(40, 0.4)	0.43	0.050	
[DMEAH][diglutarate], 60 wt %	(40, 0.4)	0.360	0.058	32
$[TETA][L]_4$, 60 wt %	(50, 3)	1.34	0.197[e]	23
CaL_2, 10 wt %	(40, 0.166)		0.014	3
L-car, 50 wt %	(40, 0.37)	0.382[c]	0.15[d]	47
Bet, 50 wt %	(40, 0.37)	0.06[c]	0.03[d]	47

[a] mol_{SO_2}/mol_{ILs}. [b] $g_{SO_2}/g_{absorbents}$. [c] $mol_{SO_2}/mol_{inner\ salts}$. [d] $g_{SO_2}/g_{inner\ salts}$. [e] g_{SO_2}/g_{ILs}.

https://dx.doi.org/10.1021/acs.iecr.0c02877
Ind. Eng. Chem. Res. 2020, 59, 16786−16794

ascribed to the stretch vibrations related to the −COOH formed after SO_2 absorption.[33,47] A new peak found at 2757 cm^{-1} was associated with the stretch vibration of −OH in −COOH.[49,50] Moreover, quantum chemical calculations were also used to provide theoretical support to the FTIR spectrum analysis (Figure 9). In further simulation calculation, we

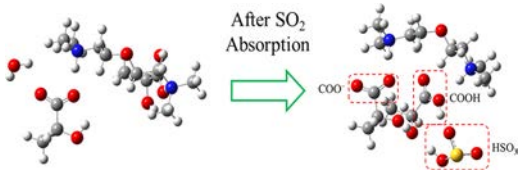

Figure 9. Optimized structures of $[BDMAEE][L]_2$ and $[BDMAEE][L]_2$-H_2SO_3 complex, scrf = (smd, solvent = water).

investigated the interaction between $[BDMAEE][L]_2$ aq and SO_2 molecule using the SMD implicit solvent model. It was observed that the strong acid (H_2SO_3) replaced a weak acid (carboxylic acid) to produce lactic acid and a new EDPIL $[BDMAEE][L][HSO_3]$. This was in agreement with the results obtained in FTIR analysis.

As shown in Figure 10, we proposed an absorption mechanism for SO_2 in line with the above analyses and

$$SO_{2(g)} \rightleftharpoons SO_{2(aq)} \quad (2)$$
$$SO_{2(aq)} + H_2O \rightleftharpoons H_2SO_3 \quad (3)$$
$$H_2SO_3 \rightleftharpoons H^+ + HSO_3^- \quad (4)$$
$$HSO_3^- \rightleftharpoons SO_3^{2-} + H^+ \quad (5)$$
$$[BDMAEE]^{2+} \rightleftharpoons [BDMAEE]^+ + H^+ \quad (6)$$
$$L^- + H^+ \rightleftharpoons LA \quad (7)$$
$$[BDMAEE]^+ + H^+ \rightleftharpoons [BDMAEE]^{2+} \quad (8)$$

Figure 10. Chemical absorption mechanism of SO_2 in 50 wt % $[BDMAEE][L]_2$ aq.

previous reports.[25,47] The sulfurous acid (H_2SO_3) originated from the dissolution and hydrolysis of SO_2. This acid underwent ionization to generate H^+, HSO_3^-, and SO_3^{2-}, and the lactate anion was protonated to form lactic acid. Moreover, based on the ionization equilibrium of the protonated amine, it was likely that $[BDMAEE]^+$ might also play a role during SO_2 absorption in aqueous solution.

3.6. Desulfurization Performance and Reversibility of $[BDMAEE][L]_2$ aq. *3.6.1. Removal Efficiency (RE) Curves of SO_2.* Figure 11 shows the removal efficiency (*RE*) of SO_2 by 2 g of 50 wt % $[BDMAEE][L]_2$ aq under different absorption conditions. The *RE* was 100% at initial absorption time, showing that all SO_2 that interacted with the absorbent was completely captured. In addition, the high removal efficiency time (*RE* > 95%) decreased from 40 to 30 min as the concentrations of SO_2 increased from 0.1 to 0.4 vol % at 40 °C. This was due to the following: according to the two-film theory, the mass transfer resistance between gas phase and gas−liquid interface mainly existed in a gas film. Moreover, the mass transfer force that drove the SO_2 molecule to diffuse through the gas film was derived from the pressure difference between the bulk gas and the gas−liquid interface. The increase in the inlet concentration of SO_2 implied that the partial pressure of SO_2 increased in the bulk gas. This significantly enhanced the mass transfer driving force and accelerated the absorption rate. Hence, the absorbent was consumed faster, resulting in the reduction of the high removal

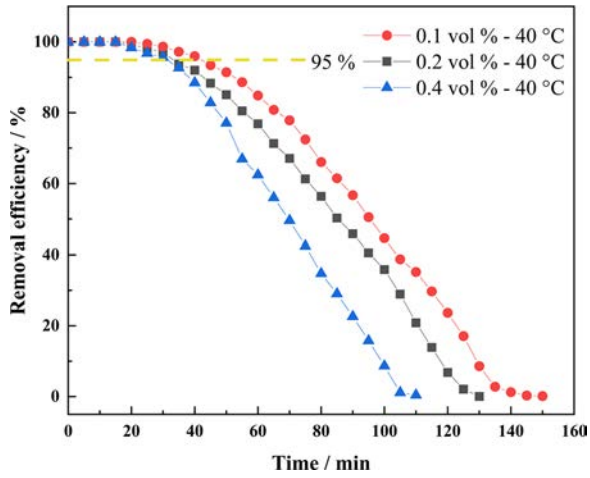

Figure 11. SO_2 removal efficiency in the 50 wt % $[BDMAEE][L]_2$ aq.

efficiency time (*RE* > 95%).[6] Compared to previously reported [DMEDA][CA] aq,[25] the absorbent synthesized in this work had a better desulfurization performance: at a high SO_2 inlet concentration, the highest *RE* of the studied absorbent reached up to 100%, and its high removal efficiency time (*RE* > 95%) was maintained at a high level for at least 30 min. The concentration of SO_2 in the flue gas is usually below 0.2 vol %, and the FGD process is generally performed in a desulfurization tower. Therefore, the desulfurization performance of the studied absorbent can be further improved by increasing the stage numbers and the flow ratios of absorbent to flue gas.

3.6.2. Reversibility of $[BDMAEE][L]_2$ aq. Reversibility is a critical parameter that determines the frequency of absorbents replacement. In this study, five cycles of SO_2 absorption−desorption experiments were carried out to investigate the reusability of the 50 wt % $[BDMAEE][L]_2$ aq. The results shown in Figure 12 demonstrated that the molar ratios of SO_2

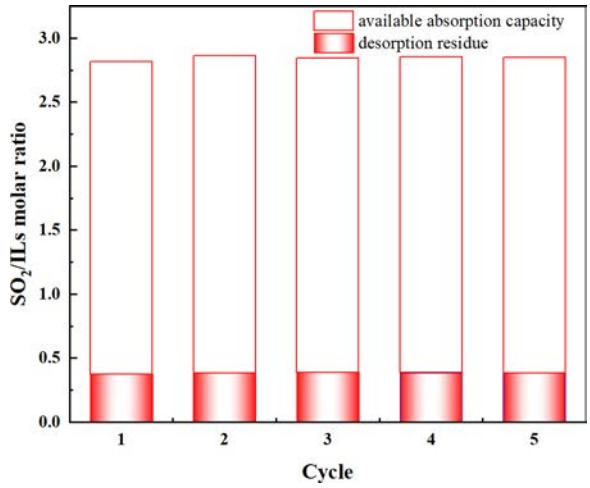

Figure 12. Reversibility of 50 wt % $[BDMAEE][L]_2$ aq.

to ILs were (2.815, 0.375), (2.863, 0.383), (2.844, 0.39), (2.852, 0.386), and (2.849, 0.385). This implied that the reversible property of the absorbent was well preserved and no notable loss of absorption capacity was observed. Thus, the absorbent synthesized in this work can be applied as a reusable absorbent in the SO_2 absorption process.

https://dx.doi.org/10.1021/acs.iecr.0c02877
Ind. Eng. Chem. Res. 2020, 59, 16786−16794

4. CONCLUSIONS

In this work, a series of novel EDPILs were designed and synthesized for efficient SO_2 absorption. By combining experimental investigations with quantum chemical calculations, we showed that EDPILs containing ether-linkage chains had higher SO_2 absorption capacities than conventional PILs. This was due to their strong physical interaction with SO_2 molecules. The application prospects of the EDPILs were promoted using an aqueous solution of $[BDMAEE][L]_2$ with the good thermostability (>148 °C). $[BDMAEE][L]_2$ aq exhibited outstanding SO_2 absorption capability and low viscosity (1.195−6.575 cP). Obviously, integration of the advantages of EDPILs and aqueous solution improved SO_2 capture. The SO_2 absorption experimental results demonstrated that the 50 wt % $[BDMAEE][L]_2$ aq efficiently absorbed SO_2 even at a low SO_2 concentration. Specifically, its absorption capacity was 1.040 mol_{SO_2}/mol_{ILs} (0.097 $g_{SO_2}/g_{absorbents}$) at 40 °C and 0.2 vol % SO_2. Based on the FTIR analysis and theoretical calculation, the mechanism of SO_2 absorption was investigated. Results revealed that the protonation of lactic acid anion significantly enhanced SO_2 dissolution and absorption. Additionally, the absorbent exhibited excellent SO_2 removal efficiency (100%) at 0.2 vol % SO_2 and 40 °C, making the absorbent applicable for large-scale applications. The novel absorbent in this study has excellent SO_2 absorption capability, outstanding reversibility, and high SO_2/CO_2 selectivity; hence, is a superior alternative to traditional absorbents for the FGD process.

■ ASSOCIATED CONTENT

Supporting Information

The Supporting Information is available free of charge at https://pubs.acs.org/doi/10.1021/acs.iecr.0c02877.

^{1}H NMR data of EDPILs; TGA curves of $[BDMAEE][L]$, $[TMEDA][L]$, and lactic acid with a 10 °C/min temperature heating rate to 800 °C under the N_2 atmosphere; the water content of the prepared PILs; details of quantum chemical calculations methods; absorption capacity of SO_2 in $[BDMAEE][L]_2$ and $[TMEDA][L]_2$ with respect to the concentration of SO_2 at 40 °C; the reaction equilibrium constant (K) and related SO_2 absorption experiments data for the absorption enthalpy calculation (the SO_2 concentration was 100 vol % and the pressure was 1 bar); the linear relationship between ln$K$ and $1/T$ for (a) $[BDMAEE][L]_2$ and (b) $[TMEDA][L]_2$; physical properties of absorbents; densities and viscosities of the studied absorbents (25 °C); SO_2/CO_2 selectivity of $[BDMAEE][L]_2$ aqueous solutions (50 wt %); and FTIR spectra in detail of 50 wt % $[BDMAEE][L]_2$ aq before (a) and after (b) absorption of SO_2 (PDF)

■ AUTHOR INFORMATION

Corresponding Author

Xiaowei Tantai − *School of Chemical Engineering and Technology, Tianjin University, Tianjin 300072, P. R. China;* orcid.org/0000-0003-2925-0444; Phone: +86 22 27400199; Email: tantaixw@tju.edu.cn

Authors

Bin Jiang − *School of Chemical Engineering and Technology, Tianjin University, Tianjin 300072, P. R. China*

Shuai Hou − *School of Chemical Engineering and Technology, Tianjin University, Tianjin 300072, P. R. China*

Luhong Zhang − *School of Chemical Engineering and Technology, Tianjin University, Tianjin 300072, P. R. China;* orcid.org/0000-0002-7073-4793

Na Yang − *School of Chemical Engineering and Technology, Tianjin University, Tianjin 300072, P. R. China;* orcid.org/0000-0003-4888-5971

Na Zhang − *School of Chemical Engineering and Technology, Tianjin University, Tianjin 300072, P. R. China*

Xiaoming Xiao − *School of Chemical Engineering and Technology, Tianjin University, Tianjin 300072, P. R. China*

Xiaodong Yang − *School of Chemical Engineering and Technology, Tianjin University, Tianjin 300072, P. R. China*

Yongli Sun − *School of Chemical Engineering and Technology, Tianjin University, Tianjin 300072, P. R. China*

Complete contact information is available at: https://pubs.acs.org/10.1021/acs.iecr.0c02877

Notes

The authors declare no competing financial interest.

■ ACKNOWLEDGMENTS

This project is financially supported by National Key R&D Program of China (no. 2016YFC0400406).

■ REFERENCES

(1) Zhang, K.; Ren, S.; Yang, X.; Hou, Y.; Wu, W.; Bao, Y. Efficient absorption of low-concentration SO_2 in simulated flue gas by functional deep eutectic solvents based on imidazole and its derivatives. *Chem. Eng. J.* **2017**, *327*, 128−134.

(2) Rahmani, F.; Mowla, D.; Karimi, G.; Golkhar, A.; Rahmatmand, B. SO_2 removal from simulated flue gas using various aqueous solutions: Absorption equilibria and operational data in a packed column. *Sep. Purif. Technol.* **2015**, *153*, 162−169.

(3) Tian, S.; Hou, Y.; Wu, W.; Ren, S.; Wang, C.; Qian, J. Reversible absorption of SO_2 from simulated flue gas by aqueous calcium lactate solution. *J. Taiwan Inst. Chem. Eng.* **2015**, *54*, 71−75.

(4) Jiang, B.; Zhang, H.; Zhang, L.; Zhang, N.; Huang, Z.; Chen, Y.; Sun, Y.; Tantai, X. Novel deep eutectic solvents for highly efficient and reversible absorption of SO_2 by preorganization strategy. *ACS Sustainable Chem. Eng.* **2019**, *7*, 8347−8357.

(5) Zhang, L.; Wu, S.; Gao, Y.; Sun, B.; Luo, Y.; Zou, H.; Chu, G.; Chen, J. Absorption of SO_2 with calcium-based solution in a rotating packed bed. *Sep. Purif. Technol.* **2019**, *214*, 148−155.

(6) Yang, J.; Gao, H.; Hu, G.; Wang, S.; Zhang, Y. Novel Process of Removal of Sulfur Dioxide by Aqueous Ammonia−Fulvic Acid Solution with Ammonia Escape Inhibition. *Energy Fuels* **2016**, *30*, 3205−3218.

(7) Zhao, T.; Li, Y.; Zhang, Y.; Wu, Y.; Hu, X. Efficient SO_2 Capture and Fixation to Cyclic Sulfites by Dual Ether-Functionalized Protic Ionic Liquids without Any Additives. *ACS Sustainable Chem. Eng.* **2018**, *6*, 10886−10895.

(8) Zhang, K.; Ren, S.; Hou, Y.; Wu, W. Efficient absorption of SO_2 with low-partial pressures by environmentally benign functional deep eutectic solvents. *J. Hazard. Mater.* **2017**, *324*, 457−463.

(9) Huang, K.; Chen, Y.-L.; Zhang, X.-M.; Xia, S.; Wu, Y.-T.; Hu, X.-B. SO_2 absorption in acid salt ionic liquids/sulfolane binary mixtures: Experimental study and thermodynamic analysis. *Chem. Eng. J.* **2014**, *237*, 478−486.

(10) Huang, J.; Ruther, T. Why are Ionic Liquids Attractive for CO_2 Absorption? An Overview. *Aust. J. Chem.* **2009**, *62*, 298−308.

(11) Zhao, W.; Chen, L.; Zhao, Q.; Chen, Y.; Zeng, Z. Liquid-solid phase-change absorption of SO_2 with tertiary diamines in long-chain alkane. *Sep. Purif. Technol.* **2019**, *229*, No. 115814.

(12) Krupiczka, R.; Rotkegel, A.; Ziobrowski, Z. Comparative study of CO_2 absorption in packed column using imidazolium based ionic liquids and MEA solution. *Sep. Purif. Technol.* **2015**, *149*, 228−236.
(13) Bhattacharyya, S.; Shah, F. U. Ether functionalized choline tethered amino acid ionic liquids for enhanced CO_2 capture. *ACS Sustainable Chem. Eng.* **2016**, *4*, 5441−5449.
(14) Sun, Y.; Ren, S.; Hou, Y.; Zhang, K.; Wu, W. Highly Efficient Absorption of NO by Dual Functional Ionic Liquids with Low Viscosity. *Ind. Eng. Chem. Res.* **2019**, *58*, 13313−13320.
(15) Cui, G.; Li, Y.; Liu, J.; Wang, H.; Li, Z.; Wang, J. Tuning Environmentally Friendly Chelate-Based Ionic Liquids for Highly Efficient and Reversible SO_2 Chemisorption. *ACS Sustainable Chem. Eng.* **2018**, *6*, 15292−15300.
(16) Vijayaraghavan, R.; Oncsik, T.; Mitschke, B.; MacFarlane, D. Base-rich diamino protic ionic liquid mixtures for enhanced CO_2 capture. *Sep. Purif. Technol.* **2018**, *196*, 27−31.
(17) Yang, D.; Hou, M.; Ning, H.; Ma, J.; Kang, X.; Zhang, J.; Han, B. Reversible capture of SO_2 through functionalized ionic liquids. *ChemSusChem* **2013**, *6*, 1191−1195.
(18) Cui, G.; Wang, C.; Zheng, J.; Guo, Y.; Luo, X.; Li, H. Highly efficient SO_2 capture by dual functionalized ionic liquids through a combination of chemical and physical absorption. *Chem. Commun.* **2012**, *48*, 2633−2635.
(19) Wang, C.; Cui, G.; Luo, X.; Xu, Y.; Li, H.; Dai, S. Highly efficient and reversible SO_2 capture by tunable azole-based ionic liquids through multiple-site chemical absorption. *J. Am. Chem. Soc.* **2011**, *133*, 11916−11919.
(20) Wu, W.; Han, B.; Gao, H.; Liu, Z.; Jiang, T.; Huang, J. Desulfurization of Flue Gas: SO_2 Absorption by an Ionic Liquid. *Angew. Chem., Int. Ed.* **2004**, *43*, 2415−2417.
(21) Shang, Y.; Li, H.; Zhang, S.; Xu, H.; Wang, Z.; Zhang, L.; Zhang, J. Guanidinium-based ionic liquids for sulfur dioxide sorption. *Chem. Eng. J.* **2011**, *175*, 324−329.
(22) Lim, S. R.; Hwang, J.; Kim, C. S.; Park, H. S.; Cheong, M.; Kim, H. S.; Lee, H. Absorption and desorption of SO_2 in aqueous solutions of diamine-based molten salts. *J. Hazard. Mater.* **2015**, *289*, 63−71.
(23) Qian, J.; Ren, S.; Tian, S.; Hou, Y.; Wang, C.; Wu, W. Highly efficient and reversible absorption of SO_2 by aqueous triethylenetetramine tetralactate solutions. *Ind. Eng. Chem. Res.* **2014**, *53*, 15207−15212.
(24) Huang, K.; Lu, J.; Wu, Y.; Hu, X.; Zhang, Z. Absorption of SO_2 in aqueous solutions of mixed hydroxylammonium dicarboxylate ionic liquids. *Chem. Eng. J.* **2013**, *215*−*216*, 36−44.
(25) Zhang, H.; Jiang, B.; Yang, N.; Zhang, N.; Zhang, L.; Huang, Z.; Xiao, X.; Tantai, X. Highly Efficient and Reversible Absorption of SO_2 from Flue Gas Using Diamino Polycarboxylate Protic Ionic Liquid Aqueous Solutions. *Energy Fuels* **2019**, *33*, 8937−8945.
(26) Ren, S.; Hou, Y.; Tian, S.; Chen, X.; Wu, W. What are functional ionic liquids for the absorption of acidic gases? *J. Phys. Chem. B* **2013**, *117*, 2482−2486.
(27) Greaves, T. L.; Drummond, C. J. Protic ionic liquids: properties and applications. *Chem. Rev.* **2008**, *108*, 206−237.
(28) Sun, Y.; Zhang, Y.; Zhang, L.; Jiang, B.; Gu, W.; Yang, H. SO_2 Capture Using pH-Buffered Aqueous Solutions of Protic Triamine-Based Ionic Liquid. *Energy Fuels* **2017**, *31*, 4193−4201.
(29) Cui, G.; Zhao, N.; Li, Y.; Wang, H.; Zhao, Y.; Li, Z.; Wang, J. Limited number of active sites strategy for improving SO_2 capture by ionic liquids with fluorinated acetylacetonate anion. *ACS Sustainable Chem. Eng.* **2017**, *5*, 7985−7992.
(30) Jiang, B.; Huang, Z.; Zhang, L.; Sun, Y.; Yang, H.; Bi, H. Highly efficient and reversible CO_2 capture by imidazolate-based ether-functionalized ionic liquids with a capture transforming process. *J. Taiwan Inst. Chem. Eng.* **2016**, *69*, 85−92.
(31) Zhang, L.; Zhang, Z.; Sun, Y.; Jiang, B.; Li, X.; Ge, X.; Wang, J. Ether-functionalized ionic liquids with low viscosity for efficient SO_2 capture. *Ind. Eng. Chem. Res.* **2013**, *52*, 16335−16340.
(32) Huang, K.; Lu, J.-F.; Wu, Y.-T.; Hu, X.-B.; Zhang, Z.-B. Absorption of SO_2 in aqueous solutions of mixed hydroxylammonium dicarboxylate ionic liquids. *Chem. Eng. J.* **2013**, *215*−*216*, 36−44.
(33) Zhang, K.; Ren, S.; Hou, Y.; Wu, W.; Bao, Y. Sodium Lactate Aqueous Solution, A Green and Stable Absorbent for Desulfurization of Flue Gas. *Ind. Eng. Chem. Res.* **2017**, *56*, 13844−13849.
(34) Yang, D.; Zhang, S.; Jiang, D.; Dai, S. SO_2 absorption in EmimCl−TEG deep eutectic solvents. *Phys. Chem. Chem. Phys.* **2018**, *20*, 15168−15173.
(35) Cao, L.; Huang, J.; Zhang, X.; Zhang, S.; Gao, J.; Zeng, S. Imidazole tailored deep eutectic solvents for CO_2 capture enhanced by hydrogen bonds. *Phys. Chem. Chem. Phys.* **2015**, *17*, 27306−27316.
(36) Sun, H.; Hunter, C. A.; Llamas, E. M. The flexibility−complementarity dichotomy in receptor−ligand interactions. *Chem. Sci.* **2015**, *6*, 1444−1453.
(37) Li, D.; Kang, Y.; Li, J.; Wang, Z.; Yan, Z.; Sheng, K. Chemically tunable DILs: Physical properties and highly efficient capture of low-concentration SO2. *Sep. Purif. Technol.* **2020**, *240*, No. 116572.
(38) Hong, S. Y.; Im, J.; Palgunadi, J.; Lee, S. D.; Lee, J. S.; Kim, H. S.; Cheong, M.; Jung, K.-D. Ether-functionalized ionic liquids as highly efficient SO_2 absorbents. *Energy Environ. Sci.* **2011**, *4*, 1802−1806.
(39) Li, J.; Kang, Y.; Li, B.; Wang, X.; Li, D. PEG-linked functionalized dicationic ionic liquids for highly efficient SO_2 capture through physical absorption. *Energy Fuels* **2018**, *32*, 12703−12710.
(40) Sonnenberg, J. H.; Ehara, M.; Toyota, M.; Fukuda, K.; Hasegawa, R.; Ishida, J.; Nakajima, M.; Honda, T.; Kitao, Y. *Gaussian 09*, revision C. 01; Gaussian, Inc: Wallingford, CT, 2009.
(41) Tian, L., version 1.8.6. http://www.keinsci.com/research/molclus.html.
(42) Wang, Y.; Wang, C.; Zhang, L.; Li, H. Difference for SO_2 and CO_2 in TGML ionic liquids: a theoretical investigation. *Phys. Chem. Chem. Phys.* **2008**, *10*, 5976−5982.
(43) Mercy, M.; de Leeuw, N. H.; Bell, R. G. Mechanisms of CO_2 capture in ionic liquids: a computational perspective. *Faraday Discuss.* **2016**, *192*, 479−492.
(44) Xu, Y.; Zhao, J.; Wu, W.; Jin, B. Experimental and theoretical studies on the influence of ionic liquids as additives on ammonia-based CO_2 capture. *Int. J. Greenhouse Gas Control* **2015**, *42*, 454−460.
(45) Damas, G.; Dias, A. B. A.; Costa, L. T. A Quantum Chemistry Study for Ionic Liquids Applied to Gas Capture and Separation. *J. Phys. Chem. B* **2014**, *118*, 9046−9064.
(46) Zhang, X.; Jiang, K.; Liu, Z.; Yao, X.; Liu, X.; Zeng, S.; Dong, K.; Zhang, S. Insight into the Performance of Acid Gas in Ionic Liquids by Molecular Simulation. *Ind. Eng. Chem. Res.* **2019**, *58*, 1443−1453.
(47) Zhang, K.; Ren, S.; Meng, L.; Hou, Y.; Wu, W.; Bao, Y. Efficient and Reversible Absorption of Sulfur Dioxide of Flue Gas by Environmentally Benign and Stable Quaternary Ammonium Inner Salts in Aqueous Solutions. *Energy Fuels* **2017**, *31*, 1786−1792.
(48) Jiang, B.; Chen, Y.; Zhang, L.; Tantai, X.; Dou, H.; Sun, Y. Design of multiple-site imidazole derivative aqueous solution for SO_2 capture in low concentration. *J. Taiwan Inst. Chem. Eng.* **2018**, *91*, 441−448.
(49) Belzner, J. "Spektroskopische Methoden in der Organischen Chemie. 5. überarbeitete Auflage. Von M. Hesse, H. Meier, B. Zeeh, Georg Thieme Verlage, Stuttgart, 1995. 364.". *Angew. Chem.* **1997**, *109*, 547.
(50) Tammer, M. Sokrates: Infrared and Raman characteristic group frequencies: tables and charts. *Colloid Polym. Sci.* **2004**, *283*, 235.

https://dx.doi.org/10.1021/acs.iecr.0c02877
Ind. Eng. Chem. Res. 2020, 59, 16786−16794